



HAL
open science

Experimental Simulation of the Volatile Hydrocarbons Generated by the Long-UV Photoprocessing of (C₆H₆) Ices with Relevance to Titan's Southern Stratospheric Ice Clouds

J. Mouzay, K. Henry, A. Ruf, I. Couturier-Tamburelli, G. Danger, N. Piétri, T. Chiavassa

► To cite this version:

J. Mouzay, K. Henry, A. Ruf, I. Couturier-Tamburelli, G. Danger, et al.. Experimental Simulation of the Volatile Hydrocarbons Generated by the Long-UV Photoprocessing of (C₆H₆) Ices with Relevance to Titan's Southern Stratospheric Ice Clouds. *The Planetary Science Journal*, 2021, 2 (1), pp.37. 10.3847/PSJ/abdd3e . hal-03330148

HAL Id: hal-03330148

<https://hal.science/hal-03330148>

Submitted on 2 Sep 2021

HAL is a multi-disciplinary open access archive for the deposit and dissemination of scientific research documents, whether they are published or not. The documents may come from teaching and research institutions in France or abroad, or from public or private research centers.

L'archive ouverte pluridisciplinaire **HAL**, est destinée au dépôt et à la diffusion de documents scientifiques de niveau recherche, publiés ou non, émanant des établissements d'enseignement et de recherche français ou étrangers, des laboratoires publics ou privés.



Distributed under a Creative Commons Attribution 4.0 International License



Experimental Simulation of the Volatile Hydrocarbons Generated by the Long-UV Photoprocessing of (C₆H₆) Ices with Relevance to Titan's Southern Stratospheric Ice Clouds

J. Mouzay¹, K. Henry¹, A. Ruf¹, I. Couturier-Tamburelli¹ , G. Danger^{1,2,3} , N. Piétri¹, and T. Chiavassa¹

¹ Aix-Marseille Université, CNRS, PIIM, UMR 7345, F-13397 Marseille, France; isabelle.couturier@univ-amu.fr, nathalie.pietri@univ-amu.fr

² Institut Universitaire de France (IUF), France

³ Aix-Marseille Université, CNRS, CNES, LAM, UMR 7326, F-13397 Marseille, France

Received 2020 February 13; revised 2021 January 12; accepted 2021 January 15; published 2021 February 25

Abstract

Ice clouds containing benzene (C₆H₆) have recently been detected in the stratosphere at the south pole of Titan. Their subsequent aging process induced by long-UV solar photons could lead to a photoreactivity that may release some volatile organic compounds in the gas phase. The characterization of this volatile organic fraction coming from the photoprocessing ($\lambda > 230$ nm) of such icy C₆H₆ has been characterized by a gas chromatograph coupled to a mass spectrometer. Complex molecular diversity is observed through the identification of C₃ to C₈ photoproducts, which belong to the alkane, alkene, and alkyne families and aromatic derivatives. Thereafter, these hydrocarbons will potentially be transported down to the surface, as condensed ices. Because the energy of solar UV photons decrease with altitude, most of these solid-state hydrocarbons will not be photochemically degraded and may contribute at the end to the organic layer that covers Titan's surface. As these materials would be probed by DraMS, the mass spectrometer on board the future Dragonfly mission, these analyses could serve as benchmarks for future molecule detection on Titan's surface.

Unified Astronomy Thesaurus concepts: [Planetary atmospheres \(1244\)](#)

1. Introduction

The atmosphere of Titan is one of the most complex environments probed by the Cassini–Huygens space mission. It supports a very diversified chemistry, the nature of which is altitude dependent (Vuitton et al. 2007; Cui et al. 2009; Coustenis et al. 2010). At high altitudes, the main atmospheric components, N₂ and CH₄, are photodissociated by energetic particles or short-wavelength solar photons that reach the upper part of the atmosphere (Yung et al. 1984; Waite et al. 2007; Coates et al. 2009; Galand et al. 2010). These reactions lead to the formation of nitrogen- and carbon-based radicals, the recombination of which results in the formation of complex organics (Samuelson et al. 1997; Coustenis et al. 2007; Imanaka & Smith 2007; Waite et al. 2007; Cui et al. 2009; Magee et al. 2009). Prior to the Cassini mission, the Infrared Interferometer and Spectrometer from the Voyager spacecraft identified several complex organics such as ethane (C₂H₆), acetylene (C₂H₂), ethylene (C₂H₄), methylacetylene (C₃H₄), propane (C₃H₈), diacetylene (C₄H₂), hydrogen cyanide (HCN), cyanoacetylene (HC₃N), and cyanogen (C₂N₂; Hanel et al. 1981; Kunde et al. 1981; Samuelson et al. 1997; Coustenis et al. 1999). Earth-based observations completed this list with the detection of benzene (C₆H₆; Coustenis et al. 2003), whose presence was confirmed in Titan's atmosphere during the Cassini–Huygens mission, both via mass spectrometry (INMS; Waite et al. 2005) and by infrared spectroscopy (CIRS; Coustenis et al. 2007), depending to the targeted altitude.

To simulate Titan's gas-phase photochemistry, experimental works have focused on the chemical composition of the

gaseous phase produced by the radio-frequency (RF)-discharged N₂/CH₄ plasma (Coll et al. 1999; Sciamma-O'Brien et al. 2010; Gautier et al. 2011; Dubois et al. 2019) relevant for the chemistry occurring in the thermosphere. Other experiments exposed these N₂/CH₄ mixtures to far-UV radiation (Tran et al. 2005; Hörst et al. 2018; Berry et al. 2019) that mimics the chemistry in the higher part of the stratosphere. The impact of a benzene addition in a far-UV-irradiated N₂/CH₄ mixture has also been experimentally investigated (Sebree et al. 2014; Yoon et al. 2014). From the binary N₂/CH₄ mixtures, the authors identified more than 35 gas-phase-produced molecules including nitrogenous derivatives, hydrocarbons, or aromatic compounds. The addition of small amounts of benzene in these N₂/CH₄ mixtures leads to a significant increase of the amount of gas-phase-detected species, which also present a higher degree of aromaticity (Yoon et al. 2014) compared to a non-benzene-containing N₂/CH₄ mixture.

Next to this experimental approach, numerical models have recently upgraded the photochemical reaction network involving benzene and highlight the potential contribution of benzene in the formation of more complex aromatic compounds such as toluene (C₆H₅CH₃), the detection of which was inferred at high altitude (Waite et al. 2007), or ethylbenzene (C₆H₅C₂H₅; Loison et al. 2019). Their respective mole fraction was estimated to be 10⁻⁶ and 10⁻⁷ around 1000 km and decreased to 10⁻⁹ and 10⁻¹⁰ at 200 km (Loison et al. 2019). The authors state that despite their weak dipolar moment, both of them could be detectable in this region, in the millimeter spectral range by the radio telescope ALMA or by infrared spectroscopy as they are IR active with resulting spectral features well separated from benzene's features. However, these two aromatics have not been detected in the lower part of Titan's atmosphere, in the stratosphere in particular.



Original content from this work may be used under the terms of the [Creative Commons Attribution 4.0 licence](#). Any further distribution of this work must maintain attribution to the author(s) and the title of the work, journal citation and DOI.

The cold temperatures in the stratosphere allow the vapor condensation of most photoproducted organics, as suggested by cloud microphysics and radiative transfer models (Lavvas et al. 2011; Barth 2017; Anderson et al. 2018). This could result in the formation of stratospheric ice clouds, whose chemical composition depends on climatic conditions that trigger variations of local temperatures as well as trace organic abundances in this part of the atmosphere (Coustenis et al. 2016; Teanby et al. 2019). Among detected organics, modeling studies determined C_6H_6 vapor condensation around 130 K at 90 km (Lavvas et al. 2011; Barth 2017) based on the temperature profile measured by the Huygens Atmospheric Structure Instrument (HASI) during the descent of the Huygens probe and on abundances measured at 33° N (flybys TB-T44; Coustenis et al. 2010). However, since 2011, exceptional climatic conditions at the south pole resulting in a drastic cooling of the stratosphere with temperatures that dropped under 120 K below 250 km were accompanied by an enrichment of vapor benzene (Coustenis et al. 2018). It contributed to the formation of several icy clouds: one in which benzene is predominantly mixed with hydrogen cyanide (Anderson et al. 2017) and another one, detected at higher stratospheric altitudes (between 168 and 278 km) (Vinatier et al. 2018), composed of benzene among other unassigned molecules. Benzene was identified via its 682 cm^{-1} signature relative to the ν_4 C–H bending mode by the CIRS instrument (Vinatier et al. 2018). A few years later, the Cassini–Huygens space mission obtained evidence of an increase of the south pole stratospheric temperatures by 10–50 K in the 210–300 km altitude range (Anderson et al. 2018; Coustenis et al. 2019). If these benzene ice clouds are long lived and are in steady state, thermal processing could occur.

In addition, Titan’s stratosphere is a low-energetic environment mainly crossed by long-UV solar photons. UV photons can penetrate farther down into the atmosphere with increasing wavelength (Clarke & Ferris 1996; Wilson 2004; Lavvas et al. 2008; Gudipati et al. 2013). The corresponding lowest altitude at which photons at each wavelength reach inside the atmosphere, with the effective optical depth $\tau_{\text{eff}} = 1$, was presented by Lavvas et al. (2008). Between 180 and 200 nm, the altitude of penetration exhibits a sharp decrease from 200 km reaching about 135 km at 200 nm. Around 100 km, photons with energies between 200 and 300 nm are absorbed. Besides, at 220 nm, the solar flux is estimated to be 1×10^{10} photons $\text{cm}^{-2} \text{ nm}^{-1} \text{ s}^{-1}$ at 200 km competing with the one obtained at the shorter wavelength in the highest atmospheric layers, which induces a complex gas-phase chemistry (Gudipati et al. 2013). Laboratory experiments have shown that these long-UV photons (180–300 nm) can alter ices as well as aerosols formed from HC_3N , HC_5N , and C_4N_2 , known to be photosensitive at these wavelengths (Gudipati et al. 2013; Couturier-Tamburelli et al. 2015, 2018a; Fleury et al. 2019). In particular, experiments on the photochemical evolution of benzene ices under UV radiations relevant for Titan’s stratosphere (Mouzay et al. 2021) demonstrate that both volatile species and a polymeric structure, whose infrared spectrum is dominated by sp^2 CH stretching modes, are produced during their processing. However, the authors only focus on the solid-phase modifications without formal assignment of the photo-products except for one of benzene’s valence isomers, fulvene.

Our experiments aim to simulate the evolution of benzene ices in the stratospheric cloud in the absence of other unidentified species observed (Vinatier et al. 2018). They give the first information on the contribution of benzene ices

exposed to long-UV solar photons in the formation of volatile species in the lower part of the atmosphere, which has never been investigated and seems of particular interest given the last observations performed by Cassini. Therefore, our experimental study suggests a first overview of the potential contribution of photoproducted benzene ices in the enhancement of trace carbonaceous organics. With gas chromatography (GC) coupled to mass spectrometry (MS), the volatile organic fraction released in the gas phase during the thermal processing of pure benzene ices irradiated under long-UV photons was characterized. Hence, this gaseous phase, enriched in hydrocarbons that have been experimentally probed, could mimic the gaseous environment of Titan’s stratosphere characterized by Cassini instruments or ground-based telescopes (ALMA). This work supplies a list of organics, most of which have not been detected in Titan’s atmosphere, that could be formed by the exposure of benzene ices to long-UV solar photons in stratospheric-like conditions and subsequently contribute to the layer of organics at the surface of Titan that will be analyzed by the future Dragonfly mission.

2. Methodology

2.1. Setup and Formation of C_6H_6 Ices

The description of the experimental setup used for these experiments is detailed elsewhere (Abou Mrad et al. 2014). Gaseous benzene (for high performance liquid chromatography (HPLC), assay $\geq 99.9\%$, from Sigma Aldrich) was deposited on a cold finger within a high vacuum chamber (10^{-8} mbar). Isolating the vacuum chamber from the pumping system to obtain a pressure near the one observed in Titan’s stratosphere is impossible because of atmospheric contaminations that could enter and stack on the frozen sample holder and may have subsequently reacted with other species or be themselves photolyzed during experiments. Each deposited ice corresponds to a quantity of 20 μmol of benzene and thickness around $0.64 \pm 0.07 \mu\text{m}$ in all samples. To estimate the ice film’s thickness (d in centimeters) in all the samples, we used the Beer–Lambert law. As in a lot of papers (Noble et al. 2012; Toumi et al. 2016; Couturier-Tamburelli et al. 2018b), we assume that our data obey the Beer–Lambert law.

The absorption coefficient, α , is defined by

$$\frac{I}{I_0} = e^{-\alpha d},$$

where I is the intensity of the transmitted light and I_0 is the intensity of the incident light and d the film thickness

So, the absorbance could be written as

$$2.303 A = \alpha d,$$

with α the absorption coefficient calculated from values tabulated in the Solid Spectroscopy Hosting Architecture of databases and the Expertises database developed by Schmitt et al. (2018).

The equation needed for the conversion is

$$\alpha = 4\pi k \tilde{\nu},$$

where k is the extinction coefficient and $\tilde{\nu}$ is the wavenumber in cm^{-1} , which implies that

$$2.303 A = 4\pi k \tilde{\nu} d.$$

The cooling of the finger is ensured by a closed-cycle helium compressor linked to a 21 CTI cold head cryostat. Temperature deposition was maintained at 130 K for few hours and then cooled down to 70 K by a resistive heater controlled by a Lakeshore 331 temperature controller. Vapor benzene deposition at 130 K, and then cooled down to 70 K, does not result in amorphous ice (see Figure A1 in Appendix A.1) but in crystalline ice (Mouzay et al. 2021), similar to the one observed in the icy south polar cloud (Vinatier et al. 2018). The evolution of ices during photolysis experiments is monitored by in situ infrared spectroscopy with a Bruker Tensor 27 Fourier Transform infrared spectrometer with a DTGS detector (Butscher et al. 2015). In addition, the presence of impurities (H_2O , CO_2) in each benzene ice film deposited is checked by IR spectroscopy, and the experiments were carried out only if the contaminations are reduced to a level below the spectrometer's limit of detection. Spectra are recorded in reflection-absorption mode in the mid-infrared region between 4000 and 600 cm^{-1} with a resolution of 1 cm^{-1} averaged over 100 scans during the photolysis experiment and 300 scans for the background. Photolysis experiments have been performed using an Oriel 500 W high-pressure mercury lamp (200–2500 nm) with discrete Hg lines in the UV–vis region between 200 and 600 nm where most of the flux (2.34×10^{16} photons $\text{cm}^{-2}\text{ s}^{-1}$; Mouzay et al. 2021) resides to simulate the photons absorbed in Titan's lower stratosphere between 90 and 200 km. During the 48 hr of photolysis, the temperature is maintained at 70 K to prevent the desorption of benzene (130 K). The duration of the photolysis was chosen according to two criteria: (1) the duration must correspond to a period of time in which benzene ices were detected in the stratosphere (here, considering a solar flux of $\sim 10^{14}$ photons $\text{cm}^{-2}\text{ s}^{-1}$ at 200 km on Titan, it corresponds to 468 days (1.3 yr) on Titan) and (2) due to the weak electronic absorption of benzene at these wavelengths, the duration must be sufficiently long to observe spectral modification using a low-sensitivity in situ technique, i.e., IR spectroscopy. After a longer duration of the photolysis step, in our experimental conditions, impurities can be trapped and participate in the photochemical activity of the ice. Photoprocessed ices are then warmed up to 300 K with the cryogenic system switched off. At 90 K, argon is added to the vacuum chamber to reach a total pressure of 5 mbar (Abou Mrad et al. 2019), which optimizes the transfer of vapor organics from the chamber toward the preconcentration loop. No modification of the photoprocessed ice is observed with IR spectroscopy after Ar addition. The species sublimating from the ice are trapped over 16 hr in a preconcentration loop cooled in liquid nitrogen (77 K). This loop is part of the interface, named Volatile Analyses from the Heating of Interstellar/cometary Ice Analogs (VAHIIA), that allows the vacuum chamber to be connected to GC-MS. A detailed description of the interface is reported elsewhere (Abou Mrad et al. 2014). Briefly, the VAHIIA interface has been developed to circumvent the impossibility of a direct injection of the volatile fraction from the vacuum chamber to the GC-MS. This interface is composed of two units: a preconcentration unit that ensures sensitivity is improved by concentrating the gas sample

via the preconcentration loop and adjusting the pressure required for its analysis by GC-MS. The second unit ensures the online injection of a specific gas volume in the GC-MS instrument. Subsequently, the preconcentration loop is warmed, inducing the passage of trapped photoproducts in the gas phase, and helium is added into the loop to reach a total pressure of 200 mbar, which facilitates the sample transfer to the injection unit of the GC-MS (Abou Mrad et al. 2014, 2016).

The photochemical evolution of benzene ices is unknown in Titan's stratospheric-like conditions. Thus, our aim is to determine which hydrocarbon can be photoproduced in a low-energy region of Titan's atmosphere that could be subsequently released in the gas phase during the changing seasons at the south pole, as it was observed a few years before at the north pole (Le Mouélic et al. 2012; Teanby et al. 2017, 2019). Due to the experimental setup used, performing irradiation at a temperature near the one at which benzene ices have been detected in the stratosphere (130 K; Vinatier et al. 2018) would have prevented the identification of some volatile species as they would have been pumped out of the cryogenic chamber. For instance, according to the condensation profile obtained at 79°S at this pole, acetylene, C_2H_2 , and diacetylene, C_4H_2 , known to be produced during the photolysis of benzene (Yokoyama et al. 1990; Varakin 2018), are expected to condense/sublime at 90 K and 120 K, respectively, in the stratosphere (Anderson et al. 2018). Because of the experimental pressure conditions, a shift of about ~ 10 K is observed between the experimental condensation point of benzene (130 K) and modeled in the stratosphere in 2015 (140 K; Anderson et al. 2018). By reporting this shift on the condensation point of C_2H_2 , in order to detect and identify this molecule, it is essential to maintain the temperature below 80 K during the photolysis. In addition, laboratory experiments that used a similar setup (high vacuum chamber) have shown that diacetylene, C_4H_2 , starts to desorb around 90 K. Therefore, we have chosen to perform photolysis experiments at 70 K.

2.2. GC-MS Conditions for Sample Analysis

To perform GC-MS analyses, we used a ThermoFisher Trace 1310 gas chromatograph coupled to a ThermoFisher ITQ 900 MS ion trap, which has been modified for gaseous sample injection. A detailed description of the setup is described elsewhere (Abou Mrad et al. 2014). A total of $500\ \mu\text{l}$ of samples were injected into a split/splitless (SSL) injector kept at 300°C operating in split mode with a ratio of 10. The GC-MS injection loop for gaseous samples is maintained at 110°C . Analytes were separated on a Rxi@-624Sil MS ($60\text{ m} \times 0.25\text{ mm i.d.} \times 1.4\ \mu\text{m}$ film thickness), using helium as carrier gas with a constant flow rate of $1.2\text{ ml minute}^{-1}$. The initial temperature of the column was set at 45°C and held for 3 minutes, followed by an increase of $5^\circ\text{C minute}^{-1}$ to 150°C and then by $20^\circ\text{C minute}^{-1}$ to a 220°C hold for 2 minutes. The transfer line to the mass spectrometer was set to 250°C . The ion source temperature was set to 250°C , and the maximum ion time in the trap is of 25 ms. The ion trap mass spectrometer worked with electronic impact as the ionization mode (ionization energy of 70 eV). The signal is collected with a full scan mode in the 15–300 u. mass range and a scan event time of 0.16 s. The resolution is 1000 at 100 amu. For these analyses, the GC has been modified with the implementation of

a MicroJet Cryo-Trap MJT-1035E from Frontier Laboratories, Ltd. on a Restek Rxi guard column (20 cm \times 0.25 mm i.d.) to enhance detection sensitivity as well as chromatographic resolution (Abou Mrad et al. 2019).

2.3. Methodology for the Semiquantitative Approach

During the photolysis, benzene polymerizes, inducing new IR features at the bottom of all benzene's absorption bands except for the one that corresponds to the $\nu_2 + \nu_{13} + \nu_{16}$ combination mode. Therefore, the benzene photolysis rate was estimated to be $14\% \pm 5\%$, $0.17 \mu\text{mol}$ determined via infrared spectroscopy by the ratio of the integrated area of the $\nu_2 + \nu_{13} + \nu_{16}$ vibrational mode peak after/before photolysis from the infrared spectra in each experiment. The quantity of benzene deposited prior to the photolysis was then multiplied by this photolysis rate to estimate the quantity of photolyzed benzene. The quantities of the compound photoproducted have been determined by integrating the areas of the chromatographic peak of the most intense ion for each selected standard. This value was extrapolated to the one resulting from the known injected quantity of the corresponding standard.

3. Results

Our previous works (Mouzay et al. 2021) demonstrated that submitted to long-UV irradiation, benzene leads to the formation of aliphatic compounds, derivative/substituted benzene compounds, and fulvene, one of benzene's valence (Figure A1 in Appendix A.1), and probably other compounds not detected in our IR spectroscopy experiments. At the end of the irradiation step, the ices are warmed up to 300 K to trap and identify the volatile organic compounds. Unfortunately, we cannot rule out that during the annealing, other products than those formed in the solid phase during the photolysis process may be formed.

3.1. Identification of Volatile Organic Compounds

Figure 1 presents the Total Ion Current (TIC) chromatogram of a pure benzene ice irradiated for 48 hr under $\lambda > 230 \text{ nm}$, followed by warming it to 300 K. Prior to the photolysis, a blank experiment was performed to identify the potential contaminations (Figure A2 in Appendix A.2). It consisted of analyzing the gas phase resulting from the warming-up of a pure non-irradiated benzene ice, using the exact same protocol without ice photolysis. Their comparison shows that numerous peaks are present on the TIC chromatogram of the irradiated ice. Therefore, an important molecular diversity has been generated by the irradiation process. To identify these volatile compounds, standards (pentane, hexane, cyclohexane, benzene, toluene, ethylbenzene, xylene isomers, and styrene) were injected in the same analytical conditions and compared to the TIC chromatogram of the irradiated ice following three parameters: the concordance of retention times, mass fragmentation patterns, and presence of the mass shift equivalent to the number of carbon atoms in the $^{13}\text{C}_6\text{H}_6$ experiment (see Figures A11–A18 in Appendix A.3). Some standards being non-available, their identification was obtained by comparing their mass spectra to the NIST database (see Figures A3–A10 in Appendix A.3).

By comparing with standards, pentane (5), hexane (7), cyclohexane (11), benzene (12), toluene (13), ethylbenzene (14), and styrene (8) were identified. Mass extraction allowed

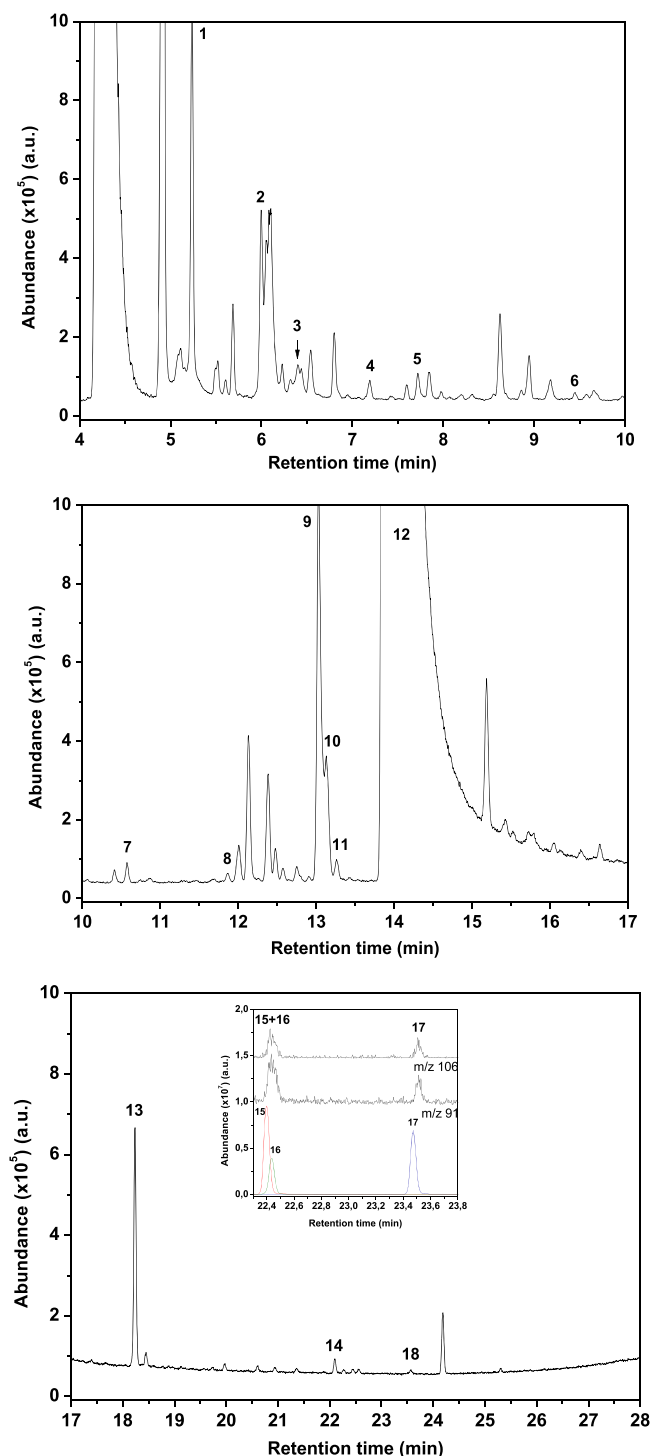


Figure 1. Total Ion Current (TIC) GC-MS chromatogram of the sublimated products of a photoproducted C_6H_6 ice. The enlarged part displays the ion extracted chromatogram of the two most intense fragments of xylene isomers (top part) and are comparable to the TIC chromatogram of the corresponding standard (bottom part): o-xylene, m-xylene, and p-xylene. The peak at 22.4 minutes (15+16) corresponds to the coelution of m- and p-xylene.

xylene isomers to be identified (insert in Figure 1). The peaks (15+16) correspond most likely to a coelution of m-xylene and p-xylene, due to their partial coelution (Table 1), while the peak (17) corresponds to the o-xylene isomer.

The comparison with the NIST database allows propene to be assigned to peak (1). Propene was already present in the C_6H_6 blank, but the ^{13}C experiment confirms its formation due

Table 1
List of Volatile Photoproducts Identified by GC-MS—Coming from the Photoprocessing of a Pure C₆H₆ Ice at 70 K Subsequently Warmed to 300 K

Products Identified	Molecular Formula	Peak Identification	Sample Rt ± E (minutes) (Peak Position in Figure 1)	Standard Rt ± E (minutes)	Identification	Relative Abundance ± E (%)	Detected in Titan's Atmosphere	Detected in Laboratory Experiments
C3 propene	C ₃ H ₆	1	5.24 ± 0.01	/	NIST	/	a	d, f, g, h, i, j
C4 but-2-ene	C ₄ H ₈	2	5.99 ± 0.01	/	NIST	/	no	d, e, f, h
but-1-en-3-yne	C ₄ H ₄	3	6.40 ± 0.02	/	NIST	/	no	d, f, h
diacetylene	C ₄ H ₂	4	7.16 ± 0.04	/	NIST	/	b	d, h, j
C5 pentane	C ₅ H ₁₂	5	7.70 ± 0.02	7.74 ± 0.02	standard	3.33 ± 0.31E−03	no	d, e, f, h, i, j
2-methyl-but-1.3-diene	C ₅ H ₈	6	9.43 ± 0.02	/	NIST	/	no	d, j
C6 hexane	C ₆ H ₁₄	7	10.6 ± 0.02	10.64 ± 0.02	standard	4.44 ± 0.04E−04	no	d, e, f, h
methylcyclopentane	C ₆ H ₁₂	8	11.9 ± 0.02	/	NIST	/	no	d
fulvene	C ₆ H ₆	9	13.0 ± 0.03	/	NIST	/	no	no
C ₆ H ₆ isomer	C ₆ H ₆	10	13.1 ± 0.05	/	NIST	/	/	/
cyclohexane	C ₆ H ₁₂	11	13.2 ± 0.02	13.26 ± 0.02	standard	2.51 ± 0.03E−04	no	d
benzene	C ₆ H ₆	12	13.9 ± 0.02	13.86 ± 0.03	standard	/	c	d, h, j
C7 toluene	C ₇ H ₈	13	18.20 ± 0.03	18.19 ± 0.01	standard	7.14 ± 0.03E−02	<i>c, inferred</i>	d, h, j
C8 ethylbenzene	C ₈ H ₁₀	14	22.10 ± 0.04	22.06 ± 0.01	standard	7.31 ± 0.17E−03	no	d
m-xylene	C ₈ H ₁₀	15 + 16	22.40 ± 0.04	22.40 ± 0.01	standard	9.64 ± 0.37E−05	no	d
p-xylene				22.44 ± 0.01	standard		no	d
o-xylene		17	23.51 ± 0.04	23.47 ± 0.01	standard	2.03 ± 0.09E−04	no	d
styrene	C ₈ H ₈	18	23.5 ± 0.04	23.54 ± 0.01	standard	5.38 ± 0.29E−03	no	d, g

Note. The quantification of selected organics is also reported, as well as retention times (Rt) of sample/standard peaks with standard error ($\pm E$, $n = 3$). The relative abundance (quantity of the selected photoproduct/quantity of C₆H₆ consumed) of each selected standard is reported. NIST corresponds to photoproducts identified by comparing their mass spectrum with the NIST database. (a): Nixon et al. (2013), (b): Kunde et al. (1981), Coustenis et al. (1991), (c): Waite et al. (2005, 2007), (d): Tran et al. (2005), (e): Coll et al. (1999), (f): Ramírez et al. (2001, 2005), (g): Jacovi et al. (2010), (h): Navarro-González et al. (2001), (i): Gautier et al. (2011), (j): Imanaka & Smith (2010).

to a mass shift of 3 of the molecular ion, as well as for other ions that present a coherent shift between the ^{12}C and ^{13}C experiments. But-2-ene may be also present at peak (2). The two most intense ions, $[\text{C}_3\text{H}_3]^+$ and $[\text{C}_3\text{H}_5]^+$ at m/z 39 and 41, respectively, of the ^{12}C mass fragmentation pattern are shifted by 3 mass units in the ^{13}C experiments; the $[\text{C}_4\text{H}_7]^+$ and $[\text{C}_4\text{H}_8]^+$ ions at m/z 55 and 56 also shift to m/z 59 and 60 in the ^{13}C experiment with the same relative intensity in each experiment. Peak (3) is assigned to but-1-en-3-yne. From the NIST database, the most intense ions are found at m/z 52 $[\text{C}_4\text{H}_4]^+$, 51 $[\text{C}_4\text{H}_3]^+$, 50 $[\text{C}_4\text{H}_2]^+$, and 49 $[\text{C}_4\text{H}]^+$ —the ions at m/z 50 and 51 presenting similar intensities. Ions from the mass spectrum of the ^{12}C experiment surrounded by a dashed blue line indicate the ones that result from the fragmentation of this compound (Figure A5 in Appendix A.3). The additional ions found below m/z 45 correspond most likely to a coelution with another unidentified compound. However, the mass fragmentation pattern from the ^{13}C experiment presents the same pattern as the ions in common with the NIST database, with a mass shift of 4 confirming the presence of four carbon atoms. Peak (4) is assigned to diacetylene. Ions from the mass spectrum of the ^{12}C experiment surrounded by a dashed blue line indicate the ones that result from the fragmentation of this compound. The other ions come from the fragmentation of other compounds, unidentified, that present a coelution with diacetylene. The comparison of this mass spectrum with the ^{13}C experiment confirms its formation during the photoprocessing of a C_6H_6 ice. Peak (6) is assigned to 2-methyl-buta-1,3-diene. The molecular ion $[\text{C}_5\text{H}_8]^+$ is shifted from m/z 68 to 73, i.e., by 5 mass units in the ^{13}C experiment; in addition, the most intense ions $[\text{C}_4\text{H}_5]^+$ and $[\text{C}_3\text{H}_3]^+$ at m/z 53 and 39 are shifted to m/z 57 and 42, respectively, by isotopic modification, which confirms this attribution. Methyl-cyclopentane is assigned to peak (8). This assignment is confirmed by the shift of the mass fragmentation pattern in the ^{13}C experiment.

Peaks (8) and (9) are assigned, respectively, to benzene isomers, as the most intense ion in the ^{12}C experiment is observed at m/z 78 and is shifted by 6 mass units in the ^{13}C experiment, indicating the presence of six carbon atoms in its structure. In our previous works (Mouzay et al. 2021), fulvene, one of benzene's isomers, has been identified by infrared spectroscopy, in both photoprocessed ($\lambda > 230$ nm) benzene ices and the cryogenic matrix in which benzene was trapped. Consequently, fulvene might correspond to the most intense peak (8), assuming equivalent ionization cross sections during the electron impact ionization between these isomers.

In addition, a peak that might correspond to the acetylene molecule is found early during the elution. To confirm this assignment, complementary analyses must be performed with another capillary column with a lower degree of polarity.

The chromatographic experiments allowed us to confirm the formation of products identified by IR spectroscopy. The absence of alkane, alkene, and alkyne absorption bands on IR spectra could be explained by the weak production rate of these other photoproducts associated with a weak infrared band strength related to their spectral features.

3.2. Semiquantification of Selected Hydrocarbons

In order to get a better understanding of the benzene photodissociation in a condition analogous to the stratosphere of Titan, a semiquantitative estimation of some identified compounds was performed. The relative abundance of photoproducts was

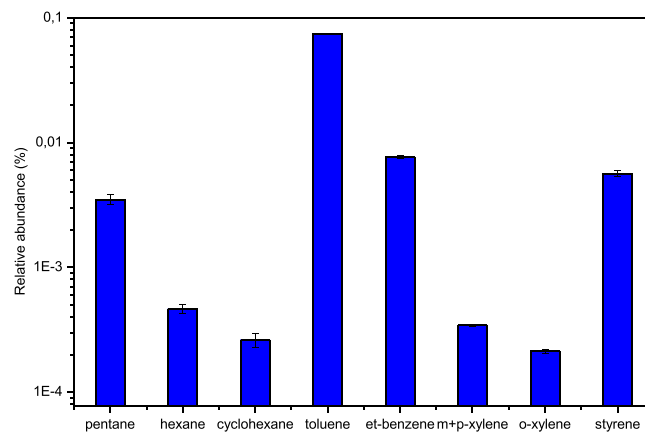


Figure 2. Relative abundances of hydrocarbons produced during the photolysis of a pure benzene ice at 70 K. Errors are calculated from replicate experiments ($n = 3$). The relative abundance of photoproducts was obtained by dividing their quantity (nmol) by the amount of benzene that was dissociated during the experiment (based on the IR spectra, $14\% \pm 5\%$, $0.17 \mu\text{mol}$).

obtained by dividing their quantity (nmol) by the amount of benzene that was dissociated during the experiment (based on the IR spectra, $14\% \pm 5\%$, $0.17 \mu\text{mol}$). As observed in Figure 2, toluene is the most abundant photoproduct in this experiment $(7.5 \pm 0.1) \times 10^{-2}\%$, followed by ethylbenzene $(7.7 \pm 0.2) \times 10^{-3}\%$, styrene $(5.6 \pm 0.3) \times 10^{-3}\%$, and pentane $(3.5 \pm 0.3) \times 10^{-3}\%$. Hexane $(4.5 \pm 0.4) \times 10^{-4}\%$, cyclohexane $(2.6 \pm 0.3) \times 10^{-4}\%$, m/p-xylene $(3.4 \pm 1.3) \times 10^{-4}\%$, and o-xylene $(2.1 \pm 0.1) \times 10^{-4}\%$ are produced with the same yield. It is interesting to notice that compounds presenting a higher number of carbons such as ethylbenzene versus toluene present a decrease in their abundances. This is in total concordance with formation via radical recombination that should lead to a decrease of abundances by at least one order of magnitude per carbon added, as previously observed in the VOC analyses coming from methanol (Abou Mrad et al. 2016). The same trend is observed for alkane families with a higher abundance of pentane than hexane.

4. Discussion

In the present study, GC-MS analyses of the volatile fraction produced during the experimental simulation of the photoprocessing of benzene ices that may occur in Titan's stratosphere, followed by warming, show a complex solid-state reactivity. From the resulting chromatogram, 17 peaks have been identified and assigned to compounds that belong either to aromatic, alkyne, alkene, or alkane families. Thus, we demonstrate that these volatile hydrocarbons can be released in the gaseous phase by the thermal processing of benzene ices previously exposed to soft UV radiation that reaches the lower part of the stratosphere. As a consequence, their formation does not result exclusively from the photochemistry of gas-phase $\text{N}_2:\text{CH}_4$ mixtures occurring in the higher part of the stratosphere to the thermosphere (Sciamma-O'Brien et al. 2010; Gautier et al. 2011; Yoon et al. 2014; Hörst et al. 2018; Berry et al. 2019; Dubois et al. 2019) but can also come from the photodegradation of ices and contribute to enhancing the chemical content of the stratospheric gas phase during the warming up of the stratosphere (Coustenis et al. 2019).

From the nadir observations performed by Cassini/CIRS in 2013 May, Vinatier et al. (2018) retrieved a C_6H_6 ice mass mixing ratio around $(1-2) \times 10^{-8}$ at ~ 100 km from 87°S to

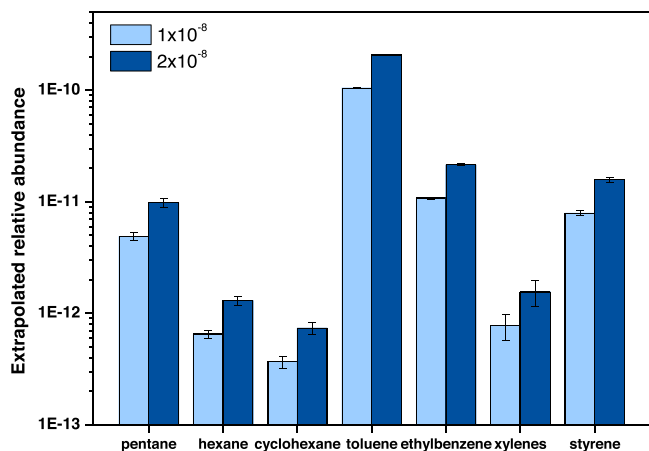


Figure 3. Relative abundances of hydrocarbons expected to be produced from the photolysis of pure benzene ice at 70 K in Titan's atmosphere. Errors are calculated from replicate experiments ($n = 3$). For the methodology of the calculation, the reader must refer to the description in the section.

65°S, thus indicating no particular latitudinal dependence. Given that the photolysis rate of benzene was estimated from our experiments at 14%, the relative quantity of photoprocessed benzene can be extrapolated to be between $1.4\% \times 10^{-9}$ and 2.8×10^{-9} at the top of the cloud in the stratosphere. Using the relative abundances of the photoproduced hydrocarbons identified in our experiments, their relative abundances were extrapolated to Titan's stratospheric conditions observed in 2013, as displayed in Figure 3. The corresponding values, with error bars, are reported in Table 2.

All hydrocarbons photoproduced have been detected as gases in our experiments subsequently to thermal processing, except for toluene, whose detection was only inferred from the INMS measurements (Waite et al. 2007), while diacetylene and propene have both been detected near 1000 km (Waite et al. 2005, 2007) and in the stratosphere with respective mixing ratios of $\sim 1 \times 10^{-9}$ at 100 km (75°S, 2013; Coustenis et al. 2016) and 2.5×10^{-9} at 225 km (Nixon et al. 2013). However, other compounds with a mixing ratio ranging from 10^{-13} to 10^{-11} are still not detected yet. For these compounds, our results allow a lower limit of their mixing ratio in the stratosphere in 2013 to be estimated. In Titan's atmosphere, the detection of hydrocarbons is provided by mass spectrometry analyses (Cassini INMS) at high altitude, but in the lower parts of the atmosphere, such as the stratosphere, their detection can only be performed by spectroscopy, which is more complex. First, in situ measurements performed by CIRS/VIMS could not have detected them as ices in significant quantities, because of the lack of sensitivity of this technique. However, despite their very weak dipolar moment (0.4 D), their detection in the millimetric wavelength range could be possible using heterodyne telescopes, such as ALMA (Loison et al. 2019), in particular for toluene and ethylbenzene that could present a molar fraction of 10^{-10} in the stratosphere. These two aromatic derivatives are the most abundant species produced during the thermal processing of photoprocessed benzene ices with an extrapolated missing ratio of 10^{-10} and 10^{-11} , respectively. Therefore, as the relative abundance of toluene in the gas phase matches the one measured in Titan's stratosphere, the photodegradation of benzene ices could be an important pathway in its production in this part of the atmosphere. However, the fact that the relative abundance of

ethylbenzene presents one order of magnitude less than the one expected in the stratosphere indicates that other pathways are involved in producing this aromatic in such relative abundance in the stratosphere.

The abundances of species resulting from photoprocessing ices under $\lambda > 230$ nm in our experiments are necessarily lower than the corresponding ones measured in Titan's atmosphere, for those that have been detected at least. Considering that the formation of such quantities of benzene ices, detected in the stratosphere, results from exceptional climatic conditions, the amount of volatile photoproducts generated by this photoprocessing ($\lambda > 230$ nm) is episodic in Titan's atmosphere. In contrast, the gas-phase photochemistry of $N_2:CH_4$ mixtures is ubiquitous and moreover more efficient, which results in the formation of higher amounts of these volatile hydrocarbons. Plus, as demonstrated in several studies, benzene photolysis was determined to be efficient only for wavelengths ranging from 165 to 220 nm (Capalbo et al. 2016; Loison et al. 2019). Here, under UV radiations at $\lambda > 230$ nm, which represents low-energy conditions, the photoabsorption of condensed benzene is very weak (Dawes et al. 2017; Mouzay et al. 2021), resulting in the calculated quantities of volatile hydrocarbons discussed above. Referring to the literature, the only study of benzene photochemical activity performed under experimental conditions closest to ours (i.e., temperature of 105 K and UV radiation at 248 nm) showed the detection of several fragments (C_6H_5 , C_2H_2 , C_2H_4 , ...) in the gas phase (Varakin 2018), which indicates that they cannot be trapped and participate in the photoreactivity. As a result, there was no decline in the nature of the volatile hydrocarbons that can be photoproduced under the conditions of Titan's lower stratosphere. As a consequence, with these considerations in mind, the detection of important chemical diversity (alkanes, alkenes, alkynes, aromatic derivatives, ...) from long-UV photoprocessed benzene ices ($\lambda > 230$ nm) performed at 70 K was not expected and can serve as a benchmark for the fate of more complex benzene ices in the low stratosphere. Thus, this study demonstrates that benzene ices detected in the stratospheric cloud at the south pole (Vinatier et al. 2018) could be a local source of hydrocarbons. They might be released in the gas phase in the stratosphere, where changing season occurs, as observed at the south pole (Coustenis et al. 2019). In addition, some of these compounds present a possible lifetime much higher than at high stratospheric altitudes or in the thermosphere/ionosphere, as long-UV photons are soft enough to prevent them from experiencing any photoinduced degradation. Therefore, these gas-phase hydrocarbons would be transported by subsidence toward lower altitudes, and thus toward colder temperatures, which would lead to their condensation resulting in ices. If the aromatic derivative precursors (toluene, ethylbenzene, xylenes) behave in the same way as their parent molecule, namely benzene, a significant amount of these ice's precursors can be pristine when they reach the surface (for benzene, only 14% of the precursor was submitted to $\lambda > 230$ nm), as the solar flux decreases with the altitude. Thus, these particles would contribute to the organic layer, which recovers either the ground or the lakes of Titan (Cordier & Carrasco 2019). Indeed, the identification of organics present on Titan's surface represents one of the main scientific objectives of the future Dragonfly space mission. This probe will be equipped with DraMS, a mass spectrometer coupled to a gas chromatograph with laser desorption as a

Table 2
Comparison of Extrapolated Experimental Mixing Ratio and In Situ Measured Mixing Ratios of Photoproduced Hydrocarbons

Identified Compounds	Formula	Relative Abundance Extrapolated in Titan's Stratospheric-like Conditions		In situ Mixing Ratio Measured in Titan's Atmosphere
Propene	C ₃ H ₆		X	2.5 × 10 ⁻⁹ (225 km) (a)
Diacetylene	C ₄ H ₂		X	1.12 × 10 ⁻⁹ (b)
Pentane	C ₅ H ₁₂	5 × 10 ⁻¹²	1 × 10 ⁻¹¹	X
Hexane	C ₆ H ₁₄	7 × 10 ⁻¹³	1 × 10 ⁻¹²	X
Cyclohexane	C ₆ H ₁₂	4 × 10 ⁻¹³	7 × 10 ⁻¹³	X
Toluene	C ₇ H ₈	1 × 10 ⁻¹⁰	2 × 10 ⁻¹⁰	<10 ⁻⁶ (1000 km) (c)
Ethylbenzene	C ₈ H ₁₀	1 × 10 ⁻¹¹	2 × 10 ⁻¹¹	X
Xylenes	C ₈ H ₁₀	8 × 10 ⁻¹³	2 × 10 ⁻¹²	X
Styrene	C ₈ H ₈	8 × 10 ⁻¹²	2 × 10 ⁻¹¹	X

References. (a) Nixon et al. (2013), (b) Coustenis et al. (2010), (c) Waite et al. (2007).

source of ionization. Because only propene, diacetylene, and toluene have been detected in Titan's atmosphere among the other hydrocarbons identified in these experiments (Kunde et al. 1981; Coustenis et al. 1991; Waite et al. 2005, 2007; Nixon et al. 2013; Table 1), this study is an exploratory work of the hydrocarbons generated in the stratosphere that could be potentially present in the organic materials analyzed at the surface of Titan during the Dragonfly mission.

Although this experimental work does not fairly reproduce the stratospheric cloud, because its complete chemical composition is still unknown and the temperature used is lower (Vinatier et al. 2018), it gives an overview of the possible volatile fraction that could be produced by the photochemical evolution of benzene ices, during a period of season changing, as observed since 2015 at the south pole (Coustenis et al. 2019). Even though pure benzene ices have not been detected and the benzene vapor mixing ratio in the south pole can be increased due to Titan's meridional circulation, some isolated ones could have been formed in the stratosphere at the same altitude range as the one at which ice clouds have been detected. This work serves as a benchmark giving preliminary results that will allow the photoprocessing of more complex ices including benzene to be studied. The determination of the influence of other organics that could have condensed with benzene will be better understood in future works, as the evolution/role of this isolated molecule was poorly known in this part of the atmosphere until now.

5. Conclusion

Laboratory experiments are crucial to prepare and analyze future space missions. In this contribution, we characterize the volatile organic fraction that is produced during the photo- and thermal processing of pure benzene ices following the recent detection of clouds that contain benzene in the southern region of Titan's stratosphere. This work is a benchmark that will allow the photochemistry of more complex ices that contain benzene, such as co-condensed ices recently detected, to be

understood. We demonstrate that long-UV photons induce the alteration of benzene ices, which generate an important molecular diversity that can be released in the gas phase, during season changes. Indeed, a GC-MS analysis of this gas phase provides the identification of alkanes (pentane, hexane), alkenes (propene, but-2-ene, 2-methylbuta-1,3-diene), alkynes (diacetylene, 1-buten-3-yne), cyclic hydrocarbons (methylcyclopentane, fulvene), and aromatic derivatives (toluene, ethylbenzene, xylene isomers, styrene). These hydrocarbons produced during the photochemical aging of benzene ices, which may occur in Titan's stratosphere, can subsequently be transported to lower altitudes via subsidence and undergo vapor condensation. As in the case of benzene, most of these compounds could be free of photochemical degradation. Hence, at the end of their sedimentation sequence that drives them toward the surface, these molecules may be present in the particles that cover Titan's surface. Given that most of the identified hydrocarbons have never been detected in the stratosphere, they might be identified in the surface organic material, which is one of the main scientific interests of the future Dragonfly space mission as a GC-MS analyzer will be dedicated to analyzing its chemical composition.

This work has been funded by the French national program "PNP," Programme de Physique et Chimie du Milieu Interstellaire (PCMI, INSU) and the Centre National d'Etudes Spatiales (CNES, exobiology program). It was also supported by the French Agence Nationale de la Recherche (VAHIA grant ANR-12-JS08-0001 and RAHIA_SSOM grant ANR-16-CE29-0015). The authors acknowledge the anonymous reviewers for helping improve this paper.

Appendix

A.1. Infrared Results

Figure A1 displays the spectra of pure benzene at different temperatures and after UV irradiation to illustrate the change in

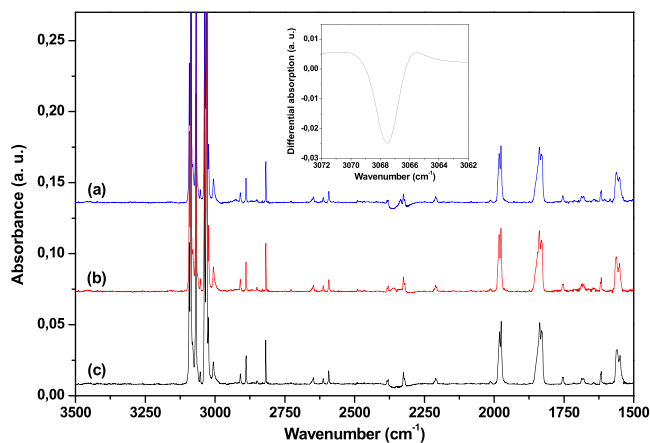


Figure A1. IR spectrum of icy benzene: (top) spectrum in the $3500\text{--}1500\text{ cm}^{-1}$ spectral range and (bottom) in the $1500\text{--}600\text{ cm}^{-1}$ spectral range focused on some of the photoproduct absorption bands (a) non-irradiated at 130 K, (b) non-irradiated after being cooled down to 70 K, and (c) after 48 hr of photolysis at 70 K under $\lambda > 230\text{ nm}$. Arrows highlight the new photoproduct spectral features corresponding to the fulvene isomer.

conditions and temperature during our experiments. These spectra provide a better understanding of the correlation between GC-MS and IR studies.

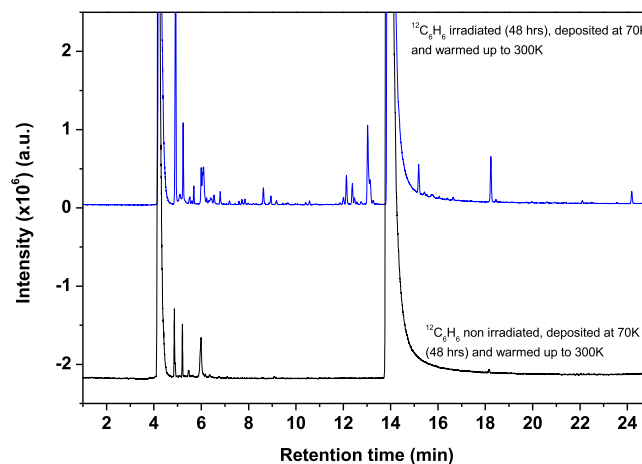


Figure A2. Comparison of the TIC chromatograms obtained after the warming of C_6H_6 ice: (top) irradiated for 48 hr at 70 K under $\lambda > 230\text{ nm}$ and (bottom) non-irradiated and maintained at 70 K for 48 hr.

A.2. 2GC-MS Results

Figure A2 shows the TIC chromatograms of a blank experiment in order to identify the potential contaminations as explained in Section 3.1.

A.3. Mass Spectroscopy Results

Figures A3–A10 represent the mass spectra of the compounds identified in the gas phase released after the warming of the photoprocessed $^{12}\text{C}_6\text{H}_6$ ice and analyzed by GC-MS. The identification methodology relies on a cross-comparison with the corresponding standards and the NIST database, supplemented by a comparison with the analytical data obtained in the $^{13}\text{C}_6\text{H}_6$ experiments, while Figures A11–A18 represent mass spectra of the compounds identified in the gas phase released after warming-up of the photoprocessed $^{12}\text{C}_6\text{H}_6$ ice and analyzed by GC-MS. For these compounds, the identification methodology relies on a comparison with the NIST database along with the analytical data obtained in the $^{13}\text{C}_6\text{H}_6$ experiments.

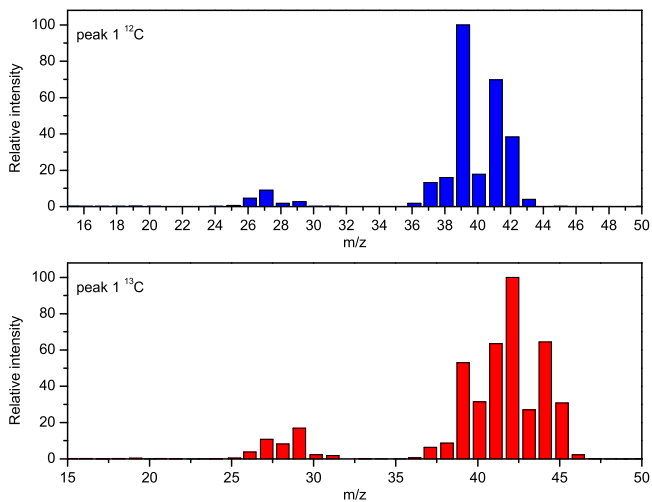


Figure A3. Mass spectrum of peak (1) assigned to propene from the ^{12}C experiment (top) compared to the one of the ^{13}C experiment (bottom).

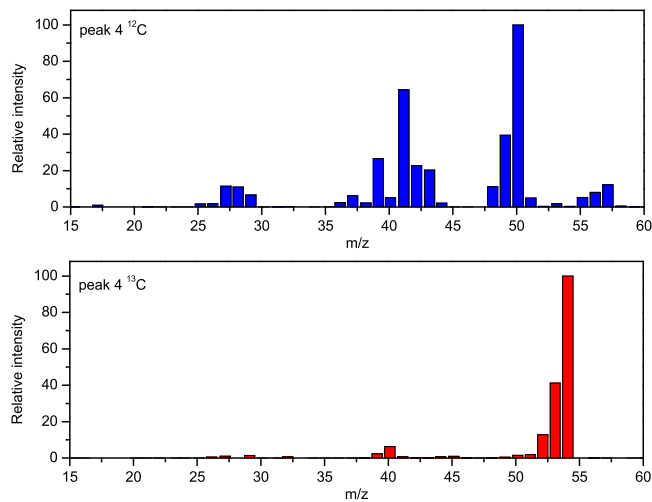


Figure A6. Mass spectrum of peak (4) assigned to diacetylene from the ^{12}C experiment (top) compared to that of the ^{13}C experiment (bottom).

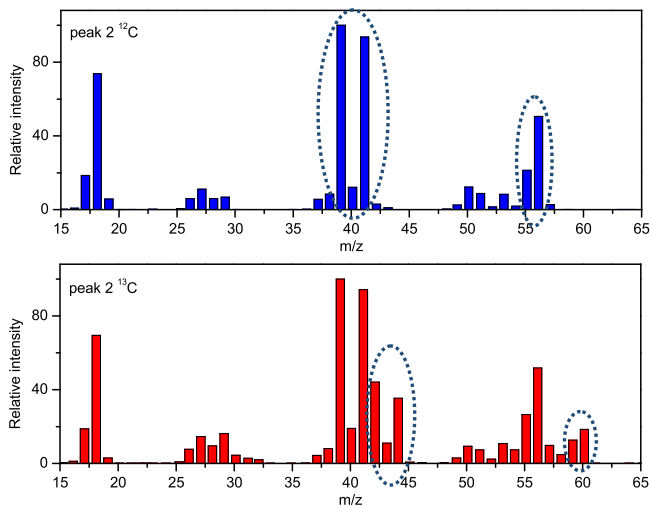


Figure A4. Mass spectrum of peak (2) assigned to but-2-ene from the ^{12}C experiment (top) compared to that of the ^{13}C experiment (bottom).

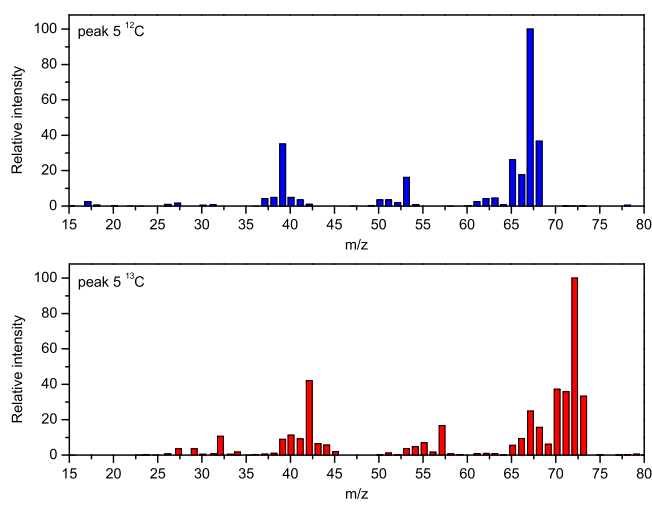


Figure A7. Mass spectrum of peak (6) assigned to 2-methyl-buta-1,3-diene from the ^{12}C experiment (top) compared to that from the ^{13}C experiment (bottom).

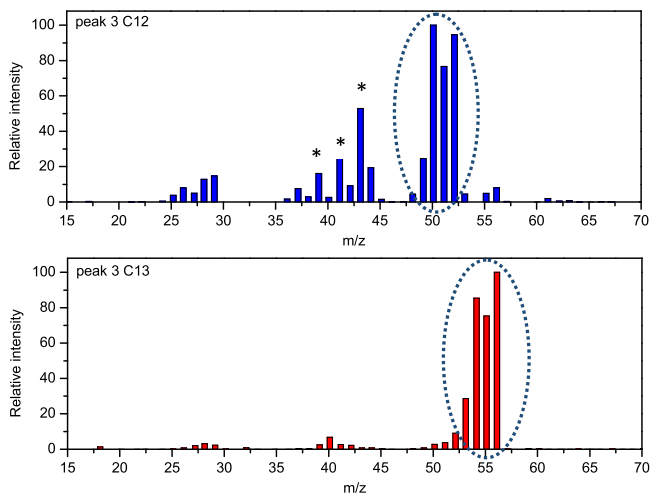


Figure A5. Mass spectrum of peak (3) assigned to but-1-en-3-yne from the ^{12}C experiment (top) compared to that of the ^{13}C experiment (bottom). * indicates ions that come from the fragmentation of another unidentified compound, which presents a coelution with but-1-en-3-yne.

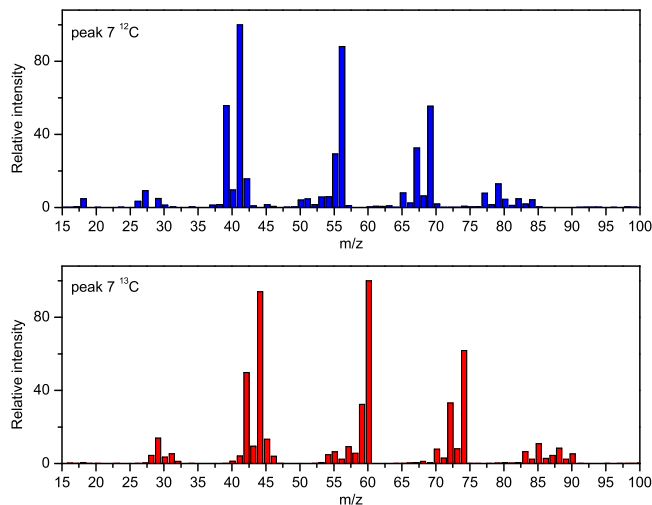


Figure A8. Mass spectrum of peak (8) assigned to methylcyclopentane from the ^{12}C experiment (top) compared to that from the ^{13}C experiment (bottom).

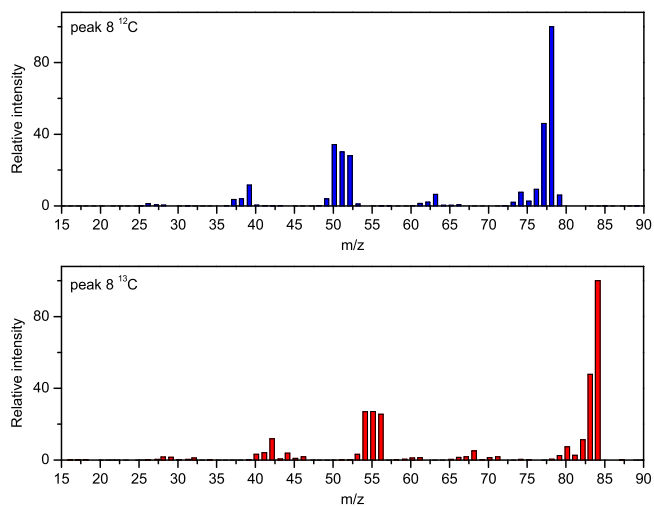


Figure A9. Mass spectrum of peak (9) assigned to fulvene from the ^{12}C experiment (top) compared to the one from the ^{13}C experiment (bottom).

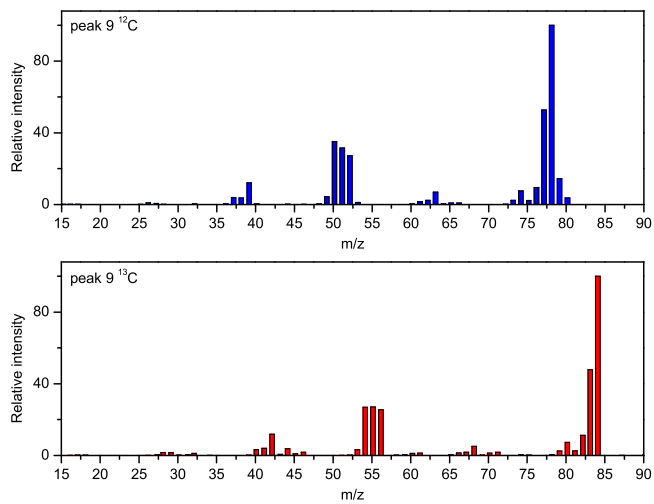


Figure A10. Mass spectrum of peak (10) assigned to another C_6H_6 valance isomer from the ^{12}C experiment (top) compared to that from the ^{13}C experiment (bottom).

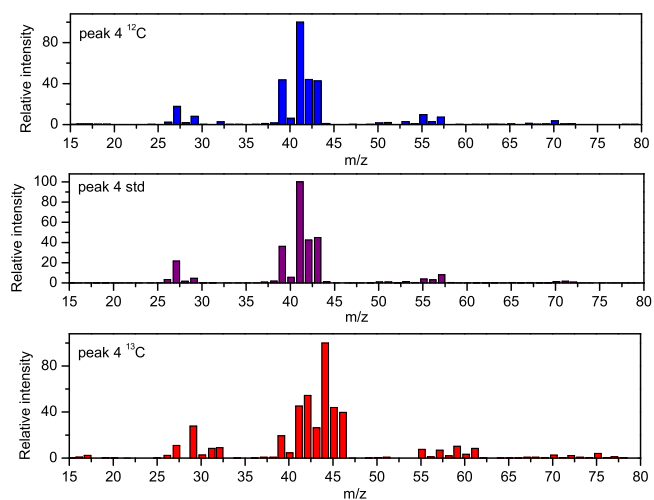


Figure A11. Mass spectrum of peak (5) assigned to pentane from the ^{12}C experiment (top) compared to that of the standard (middle) and from the ^{13}C experiment (bottom).

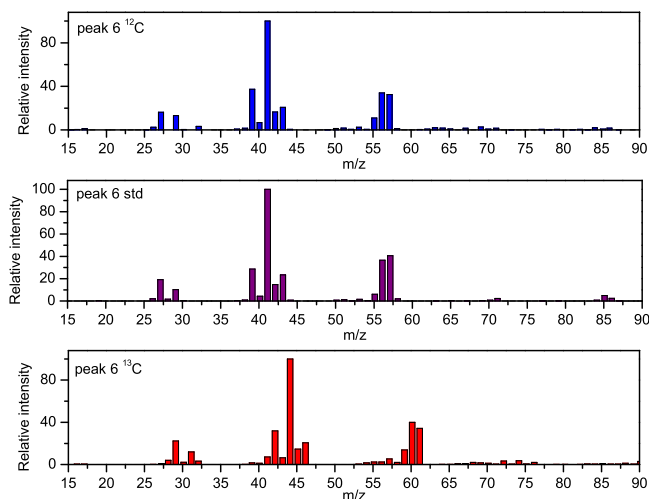


Figure A12. Mass spectrum of peak (7) assigned to hexane from the ^{12}C experiment (top) compared to that of the standard (middle) and from the ^{13}C experiment (bottom).

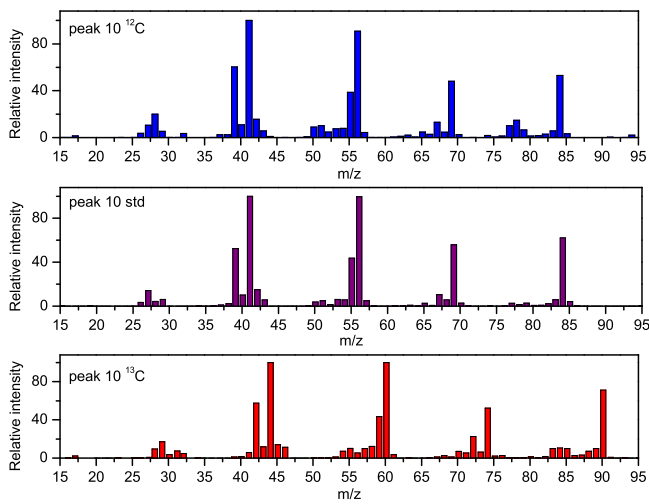


Figure A13. Mass spectrum of peak (11) assigned to cyclohexane from the ^{12}C experiment (top) compared to that of the standard (middle) and from the ^{13}C experiment (bottom).

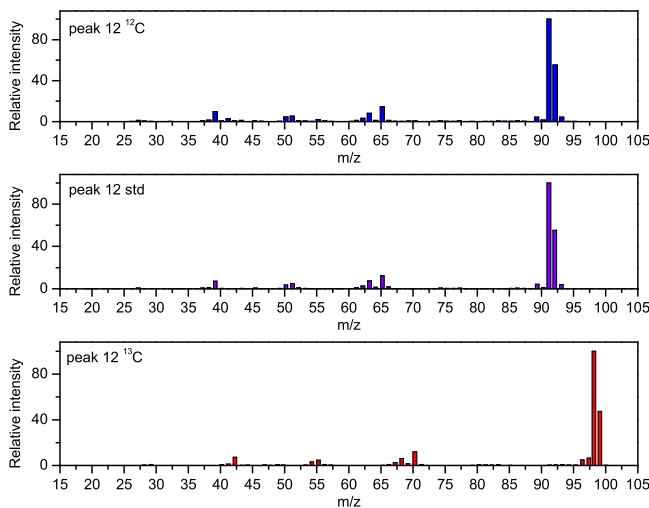


Figure A14. Mass spectrum of peak (12) assigned to toluene from the ^{12}C experiment (top) compared to that of the standard (middle) and from the ^{13}C experiment (bottom).

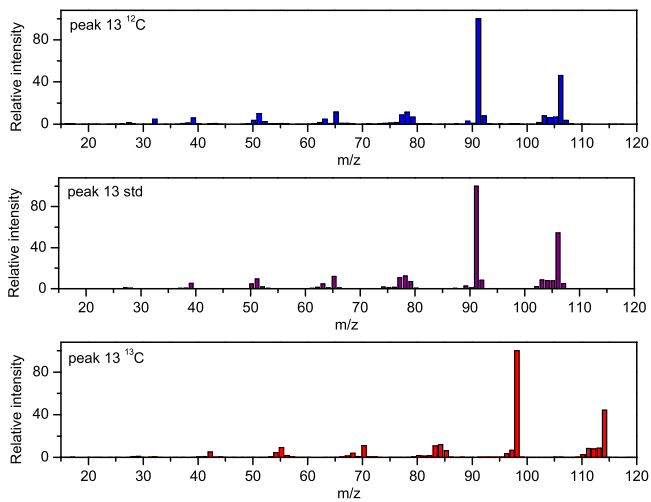


Figure A15. Mass spectrum of ethylbenzene (13) assigned to toluene from the ^{12}C experiment (top) compared to that of the standard (middle) and from the ^{13}C experiment (bottom).

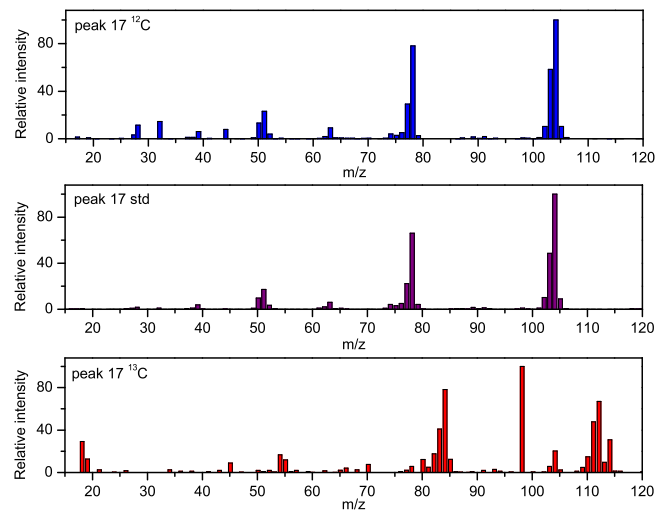


Figure A18. Mass spectrum of peak (17) assigned to styrene from the ^{12}C experiment (top) compared to that of the standard (middle) and from the ^{13}C experiment (bottom).

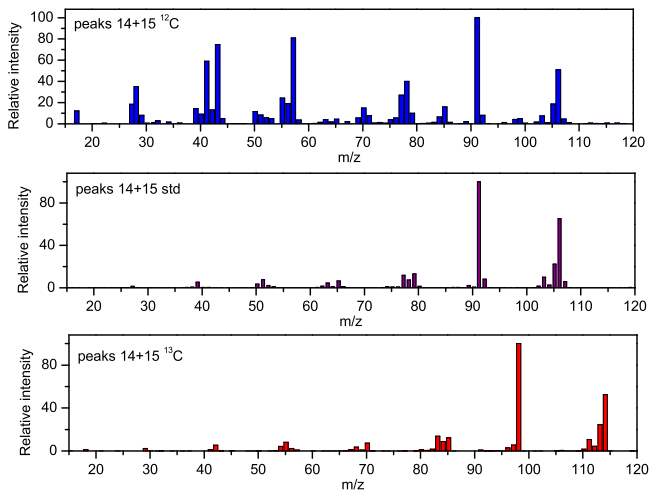


Figure A16. Mass spectrum of peaks (14+15) assigned to a coelution of m-xylene and p-xylene from the ^{12}C experiment (top) compared to that of the standard (middle) and from the ^{13}C experiment (bottom).

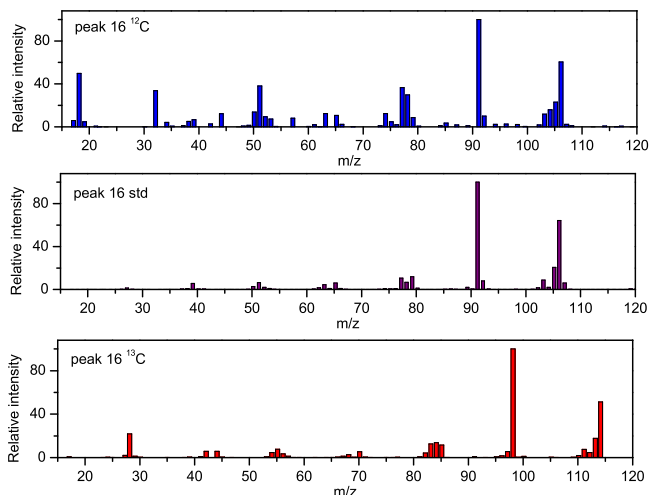


Figure A17. Mass spectrum of peak (16) assigned to o-xylene from the ^{12}C experiment (top) compared to that of the standard (middle) and from the ^{13}C experiment (bottom).

ORCID iDs

I. Couturier-Tamburelli  <https://orcid.org/0000-0002-9866-4889>

G. Danger  <https://orcid.org/0000-0002-5689-0853>

References

- Abou Mrad, N., Duvernay, F., Chiavassa, T., & Danger, G. 2016, *MNRAS*, **458**, 1234
- Abou Mrad, N., Duvernay, F., Theulé, P., Chiavassa, T., & Danger, G. 2014, *AnaCh*, **86**, 8391
- Abou Mrad, N., Werner, S., Mouzay, J., & Danger, G. 2019, *JChA*, 1609, 460489
- Anderson, C., Nna-Mvondo, D., Samuelson, R. E., et al. 2017, AAS DPS Meeting, **49**, 304.10
- Anderson, C. M., Samuelson, R. E., & Nna-Mvondo, D. 2018, *SSRv*, **214**, 125
- Barth, E. L. 2017, *P&SS*, **137**, 20
- Berry, J. L., Ugelow, M. S., Tolbert, M. A., & Browne, E. C. 2019, *ApJL*, **885**, L6
- Capalbo, F. J., Bénilan, Y., Fray, N., et al. 2016, *Icar*, **265**, 95
- Clarke, D. W., & Ferris, J. P. 1996, *JGR*, **101**, 7575
- Coates, A. J., Wellbrock, A., Lewis, G. R., et al. 2009, *P&SS*, **57**, 1866
- Coll, P., Coscia, D., Smith, N., et al. 1999, *P&SS*, **47**, 1331
- Cordier, D., & Carrasco, N. 2019, *NatGe*, **12**, 315
- Coustonis, A., Achterberg, R. K., Conrath, B. J., et al. 2007, *Icar*, **189**, 35
- Coustonis, A., Bézard, B., Gautier, D., Marten, A., & Samuelson, R. 1991, *Icar*, **89**, 152
- Coustonis, A., Jennings, D. E., Achterberg, R. K., et al. 2016, *Icar*, **270**, 409
- Coustonis, A., Jennings, D. E., Achterberg, R. K., et al. 2018, *ApJL*, **854**, L30
- Coustonis, A., Jennings, D. E., Achterberg, R. K., et al. 2019, EPSC-DPS Joint Meeting, **13**, 258
- Coustonis, A., Jennings, D. E., Nixon, C. A., et al. 2010, *Icar*, **207**, 461
- Coustonis, A., Salama, A., Schulz, B., et al. 2003, *Icar*, **161**, 383
- Coustonis, A., Schmitt, B., Khanna, R. K., & Trotta, F. 1999, *P&SS*, **47**, 1305
- Couturier-Tamburelli, I., Piétri, N., & Gudipati, M. 2015, *A&A*, **578**, A111
- Couturier-Tamburelli, I., Piétri, N., Letty, V. L., Chiavassa, T., & Gudipati, M. 2018a, *ApJ*, **852**, 117
- Couturier-Tamburelli, I., Toumi, A., Piétri, N., & Chiavassa, T. 2018b, *Icar*, **300**, 477
- Cui, J., Yelle, R. V., Vuitton, V., et al. 2009, *Icar*, **200**, 581
- Dawes, A., Pascual, N., Hoffmann, S. V., Jones, N. C., & Mason, N. J. 2017, *PCCP*, **19**, 27544
- Dubois, D., Carrasco, N., Petrucciani, M., et al. 2019, *Icar*, **317**, 182
- Fleury, B., Gudipati, M. S., Couturier-Tamburelli, I., & Carrasco, N. 2019, *Icar*, **321**, 358
- Galand, M., Yelle, R., Cui, J., et al. 2010, *JGRA*, **115**, A06314
- Gautier, T., Carrasco, N., Buch, A., et al. 2011, *Icar*, **213**, 625

- Gudipati, M. S., Jacovi, R., Couturier-Tamburelli, I., Lignell, A., & Allen, M. 2013, *NatCo*, **4**, 1648
- Hanel, R., Conrath, B., Flasar, F. M., et al. 1981, *Sci*, **212**, 192
- Hörst, S. M., Yoon, Y. H., Ugelow, M. S., Parker, A. H., & Li, R. 2018, *Icar*, **301**, 136
- Imanaka, H., & Smith, M. A. 2007, *GeoRL*, **34**, L02204
- Imanaka, H., & Smith, M. A. 2010, *PNAS*, **107**, 12423
- Jacovi, R., Laufer, D., Dimitrov, V., & Bar-Nun, A. 2010, *JGRE*, **115**, E07006
- Kunde, V. G., Aikin, A. C., Hanel, R. A., et al. 1981, *Natur*, **292**, 686
- Lavvas, P., Sander, M., Kraft, M., & Imanaka, H. 2011, *ApJ*, **728**, 80
- Lavvas, P. P., Coustenis, A., & Vardavas, I. M. 2008, *P&SS*, **56**, 67
- Le Mouélic, S., Rannou, P., Rodriguez, S., et al. 2012, *P&SS*, **60**, 86
- Loison, J. C., Dobrijevic, M., & Hickson, K. M. 2019, *Icar*, **329**, 55
- Magee, B. A., Waite, J. H., Mandt, K. E., et al. 2009, *P&SS*, **57**, 1895
- Mouzay, J., Couturier-Tamburelli, I., Pietri, N., & Chiavassa, T. 2021, *JGRE*, **126**, e2020JE006566
- Navarro-González, R., Ramírez, S. I., de la Rosa, J. G., Coll, P., & Raulin, F. 2001, *AdSpR*, **27**, 271
- Nixon, C. A., Jennings, D. E., Bézard, B., et al. 2013, *ApJL*, **776**, L14
- Noble, J. A., Theule, P., Mispelaer, F., et al. 2012, *A&A*, **543**, A5
- Ramírez, S. I., Navarro-González, R., Coll, P., & Raulin, F. 2001, *AdSpR*, **27**, 261
- Ramírez, S. I., Navarro-González, R., Coll, P., & Raulin, F. 2005, *AdSpR*, **36**, 274
- Samuelson, R. E., Nath, N. R., & Borysow, A. 1997, *P&SS*, **45**, 959
- Sciamma-O'Brien, E., Carrasco, N., Szopa, C., Buch, A., & Cernogora, G. 2010, *Icar*, **209**, 704
- Sebree, J. A., Trainer, M. G., Loeffler, M. J., & Anderson, C. M. 2014, *Icar*, **236**, 146
- Teanby, N. A., Bézard, B., Vinatier, S., et al. 2017, *NatCo*, **8**, 1586
- Teanby, N. A., Sylvestre, M., Sharkey, J., et al. 2019, *GeoRL*, **46**, 3079
- Toumi, A., Piétri, N., Chiavassa, T., & Couturier-Tamburelli, I. 2016, *Icar*, **270**, 435
- Tran, B. N., Joseph, J. C., Force, M., et al. 2005, *Icar*, **177**, 106
- Varakin, V. N. 2018, *J Photochem Photobiol Chem*, **356**, 298
- Vinatier, S., Schmitt, B., Bézard, B., et al. 2018, *Icar*, **310**, 89
- Vuitton, V., Yelle, R. V., & McEwan, M. J. 2007, *Icar*, **191**, 722
- Waite, J. H., Niemann, H., Yelle, R. V., et al. 2005, *Sci*, **308**, 982
- Waite, J. H., Young, D. T., Cravens, T. E., et al. 2007, *Sci*, **316**, 870
- Wilson, E. H. 2004, *JGRE*, **109**, E06002
- Yokoyama, A., Zhao, X., Hints, E. J., Continetti, R. E., & Lee, Y. T. 1990, *JChPh*, **92**, 4222
- Yoon, Y. H., Hörst, S. M., Hicks, R. K., et al. 2014, *Icar*, **233**, 233
- Yung, Y. L., Allen, M., & Pinto, J. P. 1984, *ApJS*, **55**, 465